

# Mitigating barren plateaus of variational quantum eigensolvers

Xia Liu,<sup>1</sup> Geng Liu,<sup>1</sup> Jiaxin Huang,<sup>1</sup> and Xin Wang<sup>1,\*</sup>

<sup>1</sup>*Institute for Quantum Computing, Baidu Research, Beijing 100193, China*

(Dated: May 27, 2022)

Variational quantum algorithms (VQAs) are expected to establish valuable applications on near-term quantum computers. However, recent works have pointed out that the performance of VQAs greatly relies on the capability of the ansatzes and is seriously limited by optimization issues such as barren plateaus (i.e., vanishing gradients). This work proposes the state efficient ansatz (SEA) for accurate quantum dynamics simulations with improved trainability. First, we show that SEA can generate an arbitrary pure state with much fewer parameters than a universal ansatz, making it efficient for tasks like ground state estimation. It also has the flexibility in adjusting the entanglement of the prepared state, which could be applied to further improve the efficiency of simulating weak entanglement. Second, we show that SEA is not a unitary 2-design even if it has universal wavefunction expressibility and thus has great potential to improve the trainability by avoiding the zone of barren plateaus. We further investigate a plethora of examples in ground state estimation and notably obtain significant improvements in the variances of derivatives and the overall optimization behaviors. This result indicates that SEA can mitigate barren plateaus by sacrificing the redundant expressibility for the target problem.

**Introduction.**— Quantum computers are expected to achieve quantum advantages [1] in solving valuable problems [2–5]. Before arriving at universal quantum computing, a key direction is to explore the power of Noisy Intermediate-Scale Quantum (NISQ) [6] devices in important fields such as quantum chemistry [7, 8] and quantum machine learning [9–13]. Recent results [14–18] have shown that quantum advantages in specific tasks can be achieved using such devices.

One common paradigm to design quantum solutions using NISQ devices is the variational quantum algorithms (VQAs) [19–21]. VQAs are promising to deliver applications in many important topics including ground state preparation [7, 8, 22], quantum data compression [23, 24], machine learning [9, 25–29], and combinatorial optimization [30, 31]. Combining the advantages of classical computers and quantum devices, VQAs adopt parameterized quantum circuits (PQCs, also known as ansatzes) [32] and utilize classical computers to optimize the parameters to minimize the cost functions that are designed for solving target problems.

Among the numerous VQAs, the variational quantum eigensolver (VQE) for ground state estimation is a central one of both practical and theoretical interests. For VQE, one common approach is to utilize fixed structure ansatzes, such as the hardware-efficient ansatz (HEA) [33] and the unitary coupled cluster (UCC) ansatz [8, 34, 35], which require a large depth to achieve high accuracy when the problem scale is large. On the other hand, there are adaptive structure ansatzes [36–40], which usually suffer from relatively high costs of both quantum and classical resources.

Despite the success of VQE, expressibility [41–43] and trainability [44–46] are still two critical challenges of designing ansatzes for VQE. To improve the accuracy of the algorithms, ansatzes with strong expressibility are usually preferred, and they are usually required to be deep enough to ensure the expressibility for finding the right solutions. This could be seen in the same spirit of deep neural networks in ma-

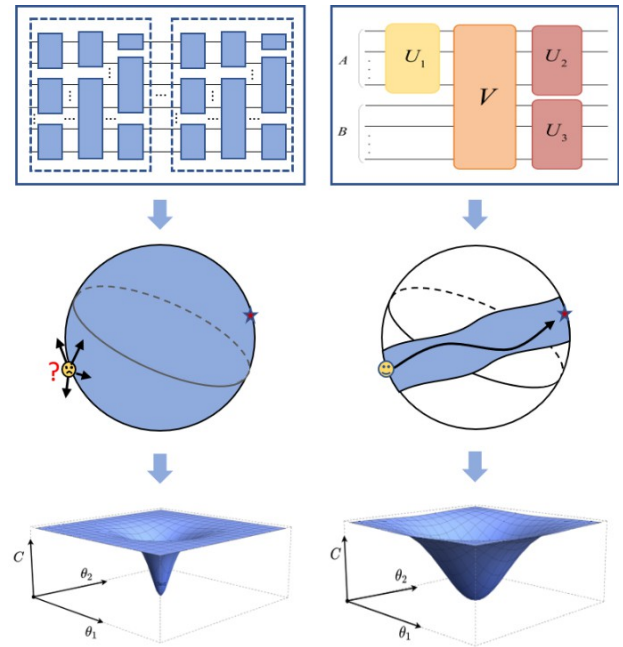


FIG. 1. **Illustration of our main result.** The left column demonstrates the difficulty in the optimization process of general ansatzes, which have high expressibility. The optimization process of State Efficient Ansatz (SEA) is depicted in the right column, with its conceptual framework represented in the upper right, where  $A$  and  $B$  are two subsystems. Schmidt coefficient layer  $U_1$ , entangling layer  $V$ , and local basis changing layer  $U_2, U_3$ , are the three parts of SEA. The key feature of SEA is reducing the optional range of paths, leading to a more favorable landscape, as shown at the bottom.

chine learning. However, recent works [43, 47, 48] have connected the expressibility and trainability implying that strong expressibility will lead to poor trainability due to the barren plateau phenomenon [44, 49, 50], i.e., the gradients in training will vanish exponentially in the number of qubits. This technical bottleneck seriously restricts the scalability of VQE. Despite a plethora of recent attempts to address the barren

\* wangxin73@baidu.com

plateaus through adjusting initialization [51, 52], cost functions [53, 54], and architectures [55], there is still a strong need for guaranteeing or extending the scalability of VQE by eliminating this trainability bottleneck while keeping the effectiveness.

To overcome these challenges, we propose the State Efficient Ansatz (SEA) to mitigate the barren plateaus and extend the scalability of VQE (see Fig. 1). We first show that SEA is effective and efficient for VQE by theoretically proving its capability of learning an arbitrary pure quantum state as well as finding the eigenstates of an arbitrary Hamiltonian. Actually, the SEA is effective for all the tasks that are essentially learning a quantum state, which we call the state-oriented tasks. We further show several useful properties of this ansatz, including its advantages in the parametric degrees of freedom as well as its flexibility in adjusting the entanglement of the prepared state. In particular, we show that SEA has the remarkable ability to mitigate the barren plateaus by removing the part of the expressibility that is redundant for generating an arbitrary pure state. We further investigate a plethora of examples in ground state estimation through numerical experiments and establish evident improvements in both the overall behavior and the variance of the partial derivatives at the initial stage.

**The State Efficient Ansatz.**— The intuition of SEA is to prune the redundant expressibility of an ansatz in the state-oriented tasks by utilizing the Schmidt representation [56] of pure states, which also inspires the tree tensor network [57–60]. Specifically, the input system has two subsystems  $A$  and  $B$ , and the ansatz comprises three parts. The first part is the *Schmidt coefficient layer*  $U_1$  acting on subsystem  $A$ . The second part is the *entangling layer*  $V$  acting on the whole system  $AB$  to create entanglement between two subsystems. The last part is the *local basis changing layer* (LBC layer), which consists of two local circuits,  $U_2$  and  $U_3$ , applied to the two subsystems respectively. The whole structure of SEA is shown in the upper right of Fig. 1 and can be written as

$$S(\theta) \equiv (U_2(\theta_2) \otimes U_3(\theta_3))V(U_1(\theta_1) \otimes I), \quad (1)$$

where  $S$  is the unitary representation of SEA,  $\theta = \{\theta_1, \theta_2, \theta_3\}$ , and each  $\theta_i$  ( $i = 1, 2, 3$ ) is a parameter vector.

We here briefly explain the effectiveness of SEA. For simplicity, we assume both subsystems  $A$  and  $B$  have  $N$  qubits and let  $|0\rangle^{\otimes 2N}$  be an initial state sent through SEA. Then  $|0\rangle^{\otimes 2N}$  will evolve into  $\sum_{k=0}^{2^N-1} \lambda_k |k\rangle_A |0\rangle_B^{\otimes N}$  ( $\lambda_k > 0$ ) after the Schmidt coefficient layer with  $U_1 |0\rangle^{\otimes N} = \sum_{k=0}^{2^N-1} \lambda_k |k\rangle_A$  (we omit  $\theta$  in writing for simplicity), where  $\{|k\rangle\}_{k=0}^{2^N-1}$  is the computational basis. At the entangling layer, we set a composition of  $N$  CNOTs controlled and targeted on the qubit-pairs  $\{(i, N+i)\}_{i=0}^{N-1}$ . After this layer, we will obtain a pure state in the form of  $\sum_{k=0}^{2^N-1} \lambda_k |k\rangle_A |k\rangle_B$ . At the last layer, we apply  $U_2$  and  $U_3$  on subsystems  $A$  and  $B$ , respectively, such that  $U_2 |k\rangle_A = |v_k\rangle_A$  and  $U_3 |k\rangle_B = |v_k\rangle_B$ . The final output state we obtain is  $\sum_{k=0}^{2^N-1} \lambda_k |v_k\rangle_A |v_k\rangle_B$ . Note that this exactly forms a Schmidt decomposition with tunable Schmidt coefficients and bases. Since any pure state has a

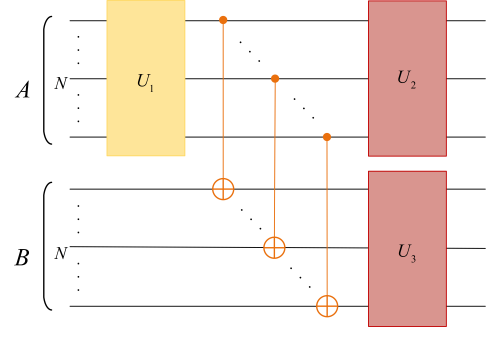


FIG. 2. **An established case of SEA.** Schmidt coefficient layer  $U_1$  has universal wavefunction expressibility. The entangling layer consists of  $N$  CNOTs, and the LBC layer comprises two local universal PQCs,  $U_2$  and  $U_3$ . The evolution of  $|0\rangle^{\otimes 2N}$  under this SEA is as follows. After Schmidt coefficient layer, we obtain  $\sum_{k=0}^{2^N-1} \lambda_k |k\rangle_A |0\rangle_B^{\otimes N}$ . Then we get  $\sum_{k=0}^{2^N-1} \lambda_k |k\rangle_A |k\rangle_B$  after implementing  $N$  CNOTs. Finally, we obtain the output state  $\sum_{k=0}^{2^N-1} \lambda_k |v_k\rangle_A |v_k\rangle_B$  after the LBC layer.

form of Schmidt decomposition, SEA can evolve an initial state  $|0\rangle^{\otimes 2N}$  into an arbitrary  $2N$ -qubit pure state if  $U_1$  can generate an arbitrary  $N$ -qubit pure state (also called *universal wavefunction expressibility*) and  $U_2, U_3$  are universal. The whole process of SEA acting on the initial state  $|0\rangle^{\otimes 2N}$  is shown in Fig. 2.

Note that not all SEA can generate an arbitrary pure state as  $\{U_i\}_{i=1}^3$  may not satisfy the conditions specified above. In the following, we consider different situations with different  $U_1$ . To simplify the study and better explore the properties of SEA, we fix the entangling layer as  $N$  CNOTs defined before (denote as  $\widetilde{\text{CNOT}}$ ), and we also assume  $U_2$  and  $U_3$  in the LBC layer are universal. We now elaborate on some useful properties of SEA with different  $U_1$ :

1. A  $2N$ -qubit SEA can evolve  $|0\rangle^{\otimes 2N}$  into an arbitrary  $2N$ -qubit pure state  $|\phi\rangle$  if  $U_1$  has universal wavefunction expressibility, as presented in Property 1.
2. The fidelity between the state evolved by SEA and a target state  $|\phi\rangle$  has a lower bound related to Schmidt rank of the target state when  $U_1$  does not have universal wavefunction expressibility, as presented in Property 2.
3. SEA has a quadratic advantage in the parametric degrees of freedom over the universal PQCs, as presented in Property 3.

We further provide detailed statements of these properties as follows, which imply the effectiveness and efficiency of SEA.

**Property 1** *If  $U_1$  can generate an arbitrary  $N$ -qubit pure state, then given any  $2N$ -qubit pure state  $|\phi\rangle$ , a  $2N$ -qubit SEA can generate  $|\phi\rangle$  with a certain set of parameters  $\hat{\theta} = \{\hat{\theta}_1, \hat{\theta}_2, \hat{\theta}_3\}$ , that is,  $S(\hat{\theta})|0\rangle^{\otimes 2N} = |\phi\rangle$ .*

Property 1 implies that SEA with a  $U_1$  of the universal wavefunction expressibility can accurately solve state-oriented tasks. Note that an  $N$ -qubit SEA under property 1

has the universal wavefunction expressibility, so we can use it as the Schmidt coefficient layer of a  $2N$ -qubit SEA to generate an arbitrary  $2N$ -qubit pure state.

However, universal wavefunction expressibility could be a strong requirement to some extent. In Property 2, we consider a relaxed condition for  $U_1$  and analyze the performance of SEA for generating an arbitrary pure state under this situation.

**Property 2** *If  $U_1$  can generate any  $N$ -qubit pure state that is a superposition of at most  $K$  computational basis states, then for any  $|\phi\rangle$ , there exists an SEA output state  $|\psi\rangle$  with  $F(|\phi\rangle, |\psi\rangle) \geq \min\{\frac{K}{r}, 1\}$ , where  $F(|\phi\rangle, |\psi\rangle)$  is the fidelity between  $|\phi\rangle$  and  $|\psi\rangle$ , and  $r$  is the Schmidt rank of  $|\phi\rangle$ .*

Property 2 states that if we know the information about entanglement of the target quantum state, we could adjust  $K$  by changing the structure of  $U_1$  to reduce the cost without sacrificing performance. Property 1 and Property 2 together show that SEA has a strong expressibility for learning a quantum state.

For a universal  $N$ -qubit PQC that can generate an arbitrary unitary, it would have at least  $O(4^N)$  parameters since the dimension of  $\mathcal{U}(2^N)$  is  $4^N$  [61]. In contrast, the Property 3 will indicate that SEA has a quadratic advantage in the parametric degrees of freedom compared to universal PQCs.

**Property 3** *Constructing a  $2N$ -qubit SEA that can generate an arbitrary pure state requires at most  $O(4^N)$  independent parameters.*

A universal  $N$ -qubit PQC  $U_i$  has  $O(4^N)$  degree of freedom [62]. Therefore, a  $2N$ -qubit SEA with universal  $U_i$  ( $i = 1, 2, 3$ ) also has  $O(4^N)$  parametric degrees of freedom. In comparison, a  $2N$ -qubit universal PQC has  $O(4^{2N})$  parametric degrees of freedom. Meanwhile, the degree of freedom of an  $N$ -qubit pure state is  $2^{N+1} - 2$ , so we do not need a universal unitary with  $O(4^N)$  parameters to generate an arbitrary state. Combining with Property 1, SEA requires quadratically fewer parameters than a general PQC of the same dimension while retaining the ability to generate an arbitrary pure state. In this sense, we call it *state efficient ansatz*. At the same time, such improvements in parameters could directly save the cost of quantum resources for measurement and introduce less noise on near-term quantum devices.

After showing the useful properties of SEA, we are going to show the validity of SEA in the variational quantum eigensolver (VQE), which aims to variationally find the ground state of a given Hamiltonian. This task plays a key role in the study of the physical and chemical properties of molecules. Combining with Property 1, we get Property 4, which illustrates the effectiveness of SEA when used in VQE.

**Property 4** *For any  $2N$ -qubit Hamiltonian  $H$ , it holds that*

$$\min_S \langle 0 |^{\otimes 2N} S^\dagger H S | 0 \rangle^{\otimes 2N} = E_0, \quad (2)$$

where  $E_0$  is the ground state energy of  $H$  and the optimization is over all unitaries reachable by SEA with  $U_1$  having universal wavefunction expressibility.

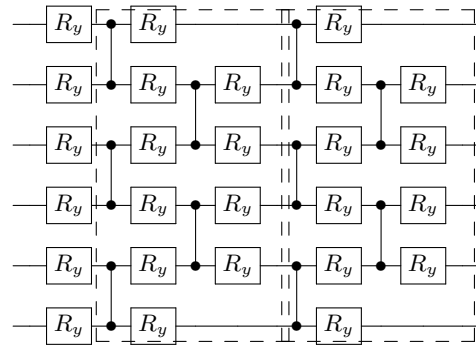


FIG. 3. An example of a 6-qubit ALT with 2 layers. Each layer is composed of the rotation operator gate  $R_y$  and control-Z gate.

Property 4 implies that SEA could be applied to search the ground state via VQE. We also note that this usually needs more resources in this situation as it may require  $U_1$  to have the universal wavefunction expressibility and  $U_2, U_3$  to be universal. To further investigate the performance in VQE, in the following parts, we choose alternating layered ansatz (ALT) [53] for the Schmidt coefficient layer and the LBC layer. An example of ALT is shown in Fig. 3.

**Applying to chemistry and physics models.**— To show the advantages of SEA, we investigate the performance of SEA and other ansatzes in estimating the ground state energy of chemistry and physics models by carrying out numerical experiments. The improvements in effectiveness and efficiency are evident. All simulations are performed using the Paddle Quantum [63] toolkit on the PaddlePaddle Deep Learning Platform [64].

**Experiment settings.** Here we use 14-qubit dinitrogen ( $N_2$ ) molecule and the 14-qubit Heisenberg model as examples for numerical simulations of VQE using SEA. As the cost of implementing a universal unitary is generally high in practice, we choose ALT as the Schmidt coefficient layer and the LBC layer to construct SEA. The structure of SEA is shown in Fig. 2, where  $U_1, U_2$ , and  $U_3$  are all 7-qubit ALTs with 30 layers. For different Hamiltonian, we could set different numbers of CNOTs in entangling layer  $V$  and different numbers of qubits of  $U_1$  in 7-qubit Schmidt coefficient layer to adjust the  $K$  in Property 2. Detailed design of  $U_1$  and  $V$  are described in *Implementation procedure*.

To study the advantages of SEA, we compare 14-qubit SEA with a 14-qubit ALT and a 14-qubit random circuit [44] in the task of VQE with a similar number of parameters by setting different depth for different ansatzes. The specific calculation methods of parameter numbers are given in the Sec. V of the Supplemental Material. The reason for choosing an ALT and a random circuit is that they both have a strong expressibility, and a random circuit can be regarded as a 2-design when its depth is large.

**Implementation procedure.** Considering that the  $N_2$  molecule and the Heisenberg model we choose are both weakly entangled, we use two kinds of SEA named SEA<sub>2</sub> and SEA<sub>3</sub> to learn these models' ground state energies. To

be specific,  $\text{SEA}_2$  is the 14-qubit SEA of Schmidt coefficient layer as a 2-qubit ALT and entangling layer as 2 CNOTs, which means a composition of 2 CNOTs controlled and targeted on the qubit-pairs  $\{(0, 7), (1, 8)\}$ .  $\text{SEA}_3$  is the 14-qubit SEA of Schmidt coefficient layer as a 3-qubit ALT and entangling layer as 3 CNOTs, which implement on the qubit-pairs  $\{(i, 7+i)\}_{i=0}^2$ . The reason we show two types of SEA is that we can implement fewer CNOTs in the entangling layer and fewer qubits in the Schmidt coefficient layer instead of  $\widetilde{\text{CNOT}}$  and  $N$ -qubit  $U_1$  in Fig. 2 to reduce entanglement. After setting up the ansatzes, we employ a stochastic gradient descent optimizer to iteratively update parameters for 400 iterations.

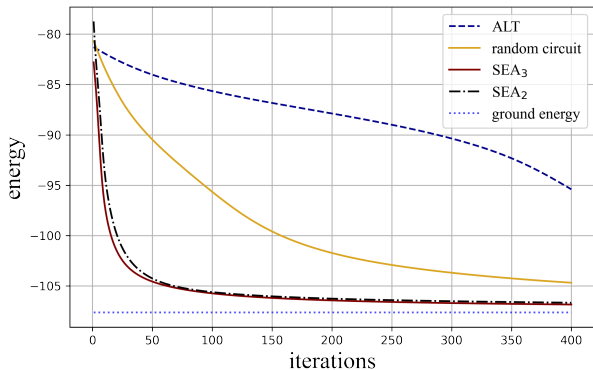


FIG. 4. **Numerical simulations of VQE on  $\text{N}_2$  (14-qubit).** The blue dotted line is the theoretical ground energy of  $\text{N}_2$ , and the lines from top to bottom represent the experimental results of ALT, the random circuit, SEA with 2 CNOTs, and SEA with 3 CNOTs, respectively.  $j$  ( $j = 2, 3$ ) CNOTs means that we set a composition of  $j$  CNOTs controlled and targeted on the qubit-pairs  $\{(i, N+i)\}_{i=0}^{j-1}$ .

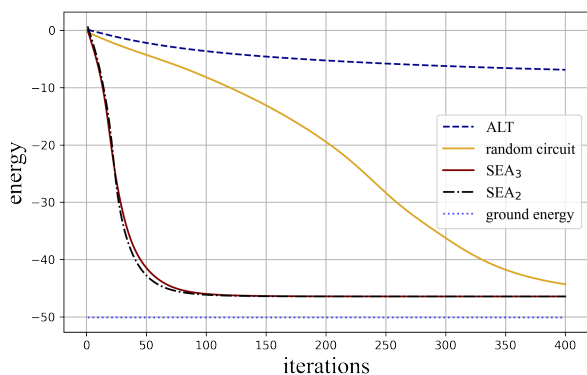


FIG. 5. **Numerical simulations of VQE on Heisenberg model (14-qubit).** The Hamiltonian is chosen to be the 14-qubit 1-dimensional spin-1/2 antiferromagnetic Heisenberg model with periodical boundary condition, i.e.,  $H = \sum_{i=1}^{14} (X_i X_{i+1} + Y_i Y_{i+1} + Z_i Z_{i+1})$ . The blue dotted line is the theoretical ground energy of the Hamiltonian  $H$ , and the other lines from top to bottom represent the results of the ALT, random circuit, SEA with 3 CNOTs and SEA with 2 CNOTs, respectively.

*Numerical results.* The simulation results of  $\text{N}_2$  molecule and the Heisenberg model are shown in Fig. 4 and Fig. 5, respectively. Both figures illustrate the efficiency of SEA on VQE. We can observe that with a similar number of parameters, there is a visible gap in the accuracy of estimating the ground energy by different ansatzes. Both  $\text{SEA}_2$  and  $\text{SEA}_3$  converge rapidly and get an approximate value of ground energy while the results of the other two ansatzes cannot be optimized in 400 iterations. In addition, it is also valid to replace the three parts of SEA with other structures. The Sec. V of the Supplemental Material presents the result of SEA whose Schmidt coefficient layer is  $R_y(\theta)^{\otimes N}$ . We can also see that this kind of SEA has better performance than ALT and random circuit, which further verifies the effectiveness of SEA in practical applications.

From the numerical experiment of VQE, we can see that SEA has an advantage in efficiency. Since we only use 2 or 3 CNOTs and adjust the structure of Schmidt coefficient layer to obtain good results, the experiment results also support Property 2.

**Mitigating Barren Plateaus.**— The evident improvement in the above VQE experiments indeed also indicates that our SEA has a good descent direction at the beginning of optimization. This fact motivates us to further study the partial derivatives of parameters at the random initialization and explore the scalability of SEA.

Trainability is one of the most concerning problems of VQAs, as it has been proved that the optimization process will be crippled because of the barren plateaus phenomenon, which means the gradients of the cost function will vanish exponentially in the number of qubits for a randomly initialized PQC. In particular, Ref. [44] has pointed out that if an ansatz can generate unitaries sufficiently randomly that accord with the Haar distribution upon unitary group up to the second moment, i.e., forms a 2-design, then the cost will exhibit a barren plateaus phenomenon. In our context, the alternating layered circuit and random circuit exhibit barren plateaus phenomenon according to our previous numeric results.

Unlike these two ansatzes that cannot find the proper descent direction, SEA does not experience a serious trainability issue at the beginning of optimization. We notably find that one main reason is that the special structure of SEA ensures it will not form a 2-design, thus mitigating the barren plateaus caused by this problem. In Theorem 1, we rigorously prove that SEA will not form a 2-design even if its local structures are 2-design.

**Theorem 1** SEA with  $U_i$  ( $i = 1, 2, 3$ ) being local 2-design and  $\widetilde{\text{CNOT}}$  as entangling layer does not form a 2-design on the global system.

A large class of random PQCs will end up forming a 2-design when the depth is large [44] and this is the usual case in VQAs. However, this theorem implies that even though the local structures of SEA have strong expressibility by forming 2-designs, which lead to the universal wavefunction expressibility of SEA according to Property 1, SEA will still not form a global 2-design. Thus SEA could avoid the known definite

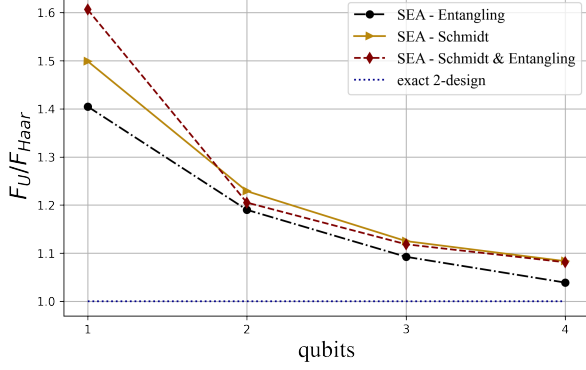


FIG. 6. **Frame potentials of 8-qubit SEA with different Schmidt coefficient layers and entangling layers.** Yellow triangles, black dots, and red diamonds represent the frame potentials of 8-qubit SEA that change the number of qubits used in the Schmidt coefficient layer, entangling layer, and both two layers, respectively. Blue dotted line represents the frame potential of an exactly 2-design circuit. Each value is estimated using an ensemble of 5000 unitaries.

zone of barren plateaus without losing effectiveness on VQE and will reveal a strong ability to mitigate the barren plateaus. Moreover, SEA will maintain this property even if we change the number of CNOTs in the entangling layer. In fact, with less expressibility, SEA will be farther from being a 2-design.

The main idea of the proof is to focus on the value of  $\langle 0|^{\otimes 2N} \int_{\mathbb{U}} U^\dagger C U \rho U^\dagger D U dU |0\rangle^{\otimes 2N}$  with  $C = D = \rho = |0\rangle\langle 0|^{\otimes 2N}$ . If a  $2N$ -qubit SEA forms a 2-design, it should hold that  $\langle 0|^{\otimes 2N} \int_{\mathbb{U}} U^\dagger C U \rho U^\dagger D U dU |0\rangle^{\otimes 2N}$  is  $\frac{2}{d^2(d^2+1)}$  with  $d = 2^N$  due to the closed form of integral formula from [65]. However, using the following Lemma 2, a key proof ingredient that explores the central structure of SEA, we find that the actual value of the target term is  $\frac{2d+6}{d^2(d+1)^3}$ . This leads to a direct contradiction as well as the fact that SEA with  $U_i (i = 1, 2, 3)$  being local 2-design structures and CNOT entangling layer does not form an exact 2-design. Even if we change the number of CNOTs in entangling layer, we can still similarly prove that SEA will not form a 2-design. We further provide the details of Theorem 1 and Lemma 2 in the Supplemental Material.

**Lemma 2** For any bipartite state  $\rho_{AB}$  with  $d_A = d_B = d$  and arbitrary linear operators  $C, D$ , we have

$$\int_{\mathcal{U}(d) \otimes \mathcal{U}(d)} d\eta(U) U^\dagger C U \rho U^\dagger D U \quad (3)$$

$$= t_0 \rho + t_1 \frac{\rho_A \otimes I_B}{d} + t_2 \frac{I_A \otimes \rho_B}{d} + t_3 I_{AB} \text{Tr}(\rho_{AB}). \quad (4)$$

where  $t_0, t_1, t_2, t_3$  are decided by  $C, D$  and dimension  $d$ .

Beyond the exact 2-design, it is natural to consider how far SEA is from being a 2-design. Here we consider the quantity called frame potential [43, 47, 48, 66], which is usually used to evaluate the randomness of an ensemble. It will reach

a minimum value if and only if the ensemble is a 2-design. The frame potential of the ensemble  $\mathbb{U}$  generated by  $2N$ -qubit SEA is denoted by  $\mathcal{F}_{\mathbb{U}}$  and the Haar value is denoted by  $\mathcal{F}_{\text{Haar}}$ . The  $\mathcal{F}_{\mathbb{U}}$  and  $\mathcal{F}_{\text{Haar}}$  are defined as follows

$$\mathcal{F}_{\mathbb{U}} = \int_{\mathbb{U}} \int_{\mathbb{U}} dU dV |\langle 0|^{\otimes 2N} (UV^\dagger) |0\rangle^{\otimes 2N}|^4, \quad (5)$$

$$\begin{aligned} \mathcal{F}_{\text{Haar}} &= \int_{\mathcal{U}(d^2)} \int_{\mathcal{U}(d^2)} d\eta(U) d\eta(V) |\langle 0|^{\otimes 2N} (UV^\dagger) |0\rangle^{\otimes 2N}|^4 \\ &= \frac{1}{(2^{2N} + 1)2^{2N-1}}, \end{aligned} \quad (6)$$

where  $U$  and  $V$  are elements of the ensemble  $\mathbb{U}$ ,  $d\eta(U)$  corresponds to the Haar measure and  $dU, dV$  correspond to the uniform distribution over  $\mathbb{U}$ . By comparing SEA with different implementations of Schmidt coefficient layer and entangling layer (cf. Fig. 6), we find that the fewer qubits used in the Schmidt coefficient layer and the fewer CNOTs in the entangling layer, the larger frame potential SEA will have, thus SEA will be farther away from being a 2-design. Therefore, when the target state is low-entangled, we can reduce the number of qubits of the Schmidt coefficient layer and the number of CNOTs in the entangling layer to further improve the trainability.

As discussed previously, SEA sacrifices some global expressibility without losing its capability to be effective on VQE. At the same time, as the trade-off of losing redundant expressibility of representing an arbitrary unitary, the special structure of SEA makes it avoid forming a 2-design, which can make it potentially mitigate the influence of barren plateaus. In particular, we can further mitigate barren plateaus by changing the specific structure of SEA according to different targets.

**Gradient experiments.**— To demonstrate that SEA can indeed mitigate the barren plateaus, we implement two numerical experiments on gradients with different numbers of qubits. For both experiments, we consider the 1-dimensional spin-1/2 antiferromagnetic Heisenberg model where the Hamiltonian is  $H = \sum_{i=1}^{2N} (X_i X_{i+1} + Y_i Y_{i+1} + Z_i Z_{i+1})$  with periodic boundary condition. We use different ansatzes and calculate the gradient of the cost function  $C(\theta) = \langle 0|^{\otimes 2N} U(\theta)^\dagger H U(\theta) |0\rangle^{\otimes 2N}$  with respect to each parameter, where  $U(\theta)$  represents the unitary of the ansatz.

**SEA with ALT.** We first conduct experiments with the ansatzes used in the previous numerical simulations of VQE. The SEAs we chose are  $\text{SEA}_1$  and  $\text{SEA}_{\lfloor N/2 \rfloor}$ , which still adopt ALT as the Schmidt coefficient layer and the LBC layer. ALT and random circuit of the same size as SEAs are selected for comparison.

The average variances of parameters of different ansatzes are compared in Fig. 7. We also extract the variance of the largest partial derivative in each sample, which is shown in the Sec. V of the Supplemental Material. It is clearly demonstrated that all these variances decay exponentially as the number of qubits increases. However, the slopes of the red and the blue lines are nearly half of the slopes of the other lines, which means the SEA has a much lower rate of decay of variance.

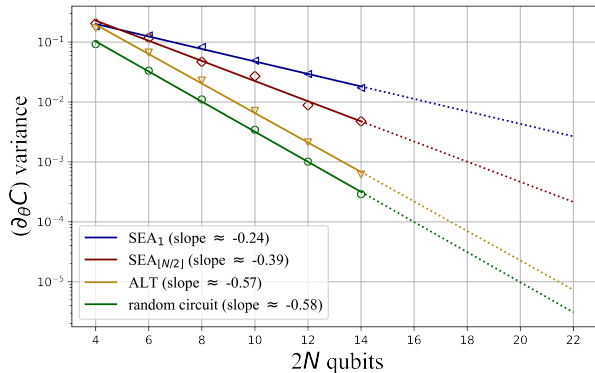


FIG. 7. **Comparison of the scaling of the average variance of gradients between different ansatzes on the Heisenberg model.** This shows the semi-log plot of the average value of the variance of each parameters in the circuit. The depth of each part of SEA is 30 and we ensure different ansatzes have similar numbers of parameters by setting different depth. The solid part of the fitted lines represents the range we experiment with, while the dashed part represents the expected performance on a larger range.

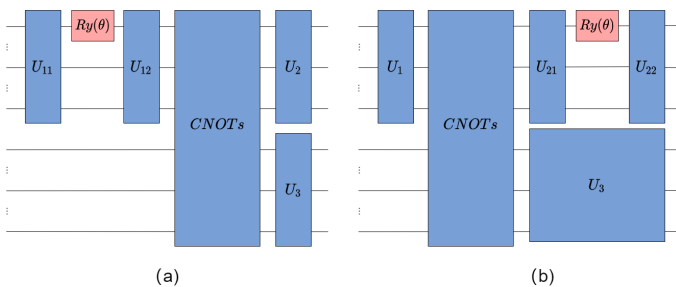


FIG. 8. **The structures of SEA used for studying the scaling of variance of general circuits** Panel (a) shows the  $R_y$  gate located in Schmidt coefficient layer. Panel (b) shows the  $R_y$  gate located in the LBC layer. Parameter  $\theta \in [0, 2\pi)$  is uniformly chosen and  $U_1, U_{11}, U_{12}, U_2, U_{21}, U_{22}, U_3$  are Haar randomly chosen from unitary group in each round of sampling.  $CNOTs$  is composed by a number of CNOTs.

*SEA with general circuits.* To better illustrate how our structure increases the scaling of variance, we further inspect the gradient with respect to the parameter in different parts of SEA. As shown in Fig. 8, we look into the gradients with respect to the parameters of the  $R_y$  gates in the Schmidt coefficient layer and the LBC layer. As a comparison, we also consider a single parameter  $R_y$  gate in the middle of a circuit that forms a 2-design with sufficient depth. The circuit before the gate and the circuit after the gate are both 2-design and are represented by Haar random unitaries in our experiments. Fig. 9 summarizes the results of the variance of parameters located in the Schmidt coefficient layer and the LBC layer, respectively.

From Fig. 9, we see that no matter where this parameter is located in SEA, the variance of its gradient has a decaying speed lower than the decay speed of variance of the pa-

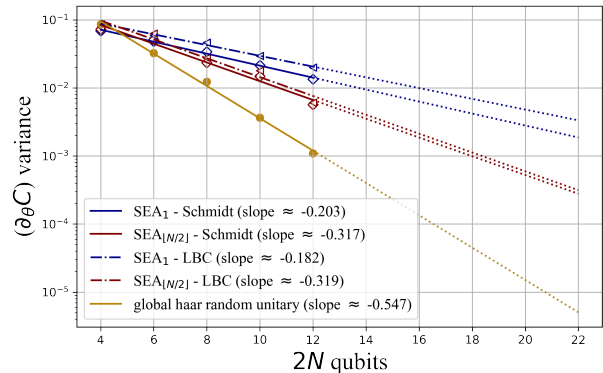


FIG. 9. **Comparison of the scaling of variance between general structure of SEA and general random circuit.** The  $SEA_1$ -Schmidt and the  $SEA_{[N/2]}$ -Schmidt show the semi-log plot of the variance of gradient with respect to the parameter in Schmidt coefficient layer. The  $SEA_1$ -LBC and the  $SEA_{[N/2]}$ -LBC show the semi-log plot of the variance of gradient with respect to the parameter in LBC layer. The markers on the fitted lines represent the results from our experiments. The dotted part of the lines represents the expected performance on a larger range.

parameter in a sufficiently random circuit that forms a 2-design. This fact indicates that the variance of SEA has significant improvement compared to using an ansatz that forms a 2-design, indicating an evident mitigation of barren plateaus. It is also worth noting that the fewer CNOTs in the entangling layer, the larger variance it will have. Specifically, in our experiments, if the scale of the problem is larger than 12 qubits, the variance of the gradients in a 2-design circuit will be less than  $10^{-3}$ , which is usually considered too small to be further optimized. However, this bound of scale can be increased to 18 qubits using SEA with  $\lfloor \frac{N}{2} \rfloor$  CNOTs according to our experiment results. With the weaker expressibility of SEA, this bound can be further increased. In other words, we can notably increase the scale of problems with the same limited scaling of gradients by using SEA instead of a 2-design circuit. Therefore, SEA is more likely to scale to larger systems on VQE tasks because of its improvement in trainability by mitigating barren plateaus.

**Concluding remarks.**— The main contribution of this work is proposing an ansatz structure SEA to mitigate the barren plateaus in optimizing parameterized circuits for quantum dynamics simulations. We in particular have provided an explicit construction of SEA that has enough expressibility to generate arbitrary pure quantum states while not forming a unitary 2-design. We have shown that SEA can be applied to approximate the ground state of the  $N_2$  molecule and the Heisenberg model, whose numerical results confirm the effectiveness of SEA. We further compare the scaling of variance in partial derivatives between different ansatzes and establish that SEA has a much lower rate of decay of variance, implying that SEA can considerably mitigate the barren plateaus of VQE. This advantage in trainability mainly comes from the elimination or sacrifice of redundant expressibility.

We note that SEA is also effective in principle for other tasks with the sole purpose of generating a pure state, e.g., combinatorial optimization [67] and entanglement detection [68]. It is natural to explore how to extend our structure by considering multipartite systems and other possible designs. We also remark that there are other proposals for dealing with barren plateaus [40, 69–71], and for using meta-learning to improve efficiency [72–75]. The combination between SEA and other approaches such as adaptive methods

may be worth a future study. Moreover, there are recent works exploiting the symmetry of VQAs [76–78], it is also worth studying how to improve the performance of SEA through the perspective of symmetry.

**Acknowledgements.** X. L. and G. L. contributed equally to this work. Part of this work was done when X. L., G. L., and J. H. were interns at Baidu Research. We would like to thank Runyao Duan, Yin Mo, Chengkai Zhu, and Youle Wang for helpful discussions.

- 
- [1] J. Preskill, arXiv preprint arXiv:1203.5813 (2012).
- [2] S. Lloyd, *Science* **273**, 1073 (1996).
- [3] A. W. Harrow, A. Hassidim, and S. Lloyd, *Physical review letters* **103**, 150502 (2009).
- [4] A. M. Childs and W. van Dam, *Reviews of Modern Physics* **82**, 1 (2010).
- [5] A. Montanaro, *npj Quantum Information* **2**, 15023 (2016).
- [6] J. Preskill, *Quantum* **2**, 79 (2018).
- [7] Y. Cao, J. Romero, J. P. Olson, M. Degroote, P. D. Johnson, M. Kieferová, I. D. Kivlichan, T. Menke, B. Peropadre, N. P. Sawaya, *et al.*, *Chemical reviews* **119**, 10856 (2019).
- [8] S. McArdle, S. Endo, A. Aspuru-Guzik, S. C. Benjamin, and X. Yuan, *Reviews of Modern Physics* **92**, 015003 (2020).
- [9] M. Schuld and F. Petruccione, *Machine Learning with Quantum Computers* (2021).
- [10] J. Biamonte, P. Wittek, N. Pancotti, P. Rebentrost, N. Wiebe, and S. Lloyd, *Nature* **549**, 195 (2017).
- [11] H.-Y. Huang, R. Kueng, G. Torlai, V. V. Albert, and J. Preskill, arXiv:2106.12627, 1 (2021), arXiv:2106.12627.
- [12] S. Jerbi, L. J. Fiderer, H. P. Nautrup, J. M. Kübler, H. J. Briegel, and V. Dunjko, arXiv:2110.13162, 1 (2021), arXiv:2110.13162.
- [13] K. Mitarai, M. Negoro, M. Kitagawa, and K. Fujii, *Physical Review A* **98**, 032309 (2018), arXiv:1803.00745.
- [14] F. Arute, K. Arya, R. Babbush, D. Bacon, J. C. Bardin, R. Barends, R. Biswas, S. Boixo, F. G. Brandao, D. A. Buell, *et al.*, *Nature* **574**, 505 (2019).
- [15] Y. Wu, W.-S. Bao, S. Cao, F. Chen, M.-C. Chen, X. Chen, T.-H. Chung, H. Deng, Y. Du, D. Fan, M. Gong, C. Guo, C. Guo, S. Guo, L. Han, L. Hong, H.-L. Huang, Y.-H. Huo, L. Li, N. Li, S. Li, Y. Li, F. Liang, C. Lin, J. Lin, H. Qian, D. Qiao, H. Rong, H. Su, L. Sun, L. Wang, S. Wang, D. Wu, Y. Xu, K. Yan, W. Yang, Y. Yang, Y. Ye, J. Yin, C. Ying, J. Yu, C. Zha, C. Zhang, H. Zhang, K. Zhang, Y. Zhang, H. Zhao, Y. Zhao, L. Zhou, Q. Zhu, C.-Y. Lu, C.-Z. Peng, X. Zhu, and J.-W. Pan, *Physical Review Letters* **127**, 180501 (2021).
- [16] H.-S. Zhong, H. Wang, Y.-H. Deng, M.-C. Chen, L.-C. Peng, Y.-H. Luo, J. Qin, D. Wu, X. Ding, Y. Hu, P. Hu, X.-Y. Yang, W.-J. Zhang, H. Li, Y. Li, X. Jiang, L. Gan, G. Yang, L. You, Z. Wang, L. Li, N.-L. Liu, C.-Y. Lu, and J.-W. Pan, *Science* **370**, 1460 (2020).
- [17] H.-S. Zhong, Y.-H. Deng, J. Qin, H. Wang, M.-C. Chen, L.-C. Peng, Y.-H. Luo, D. Wu, S.-Q. Gong, H. Su, *et al.*, *Physical review letters* **127**, 180502 (2021).
- [18] A. Abbas, D. Sutter, C. Zoufal, A. Lucchi, A. Figalli, and S. Woerner, *Nature Computational Science* **1**, 403 (2021), arXiv:2011.00027.
- [19] M. Cerezo, A. Arrasmith, R. Babbush, S. C. Benjamin, S. Endo, K. Fujii, J. R. McClean, K. Mitarai, X. Yuan, L. Cincio, *et al.*, *Nature Reviews Physics* **3**, 625 (2021).
- [20] K. Bharti, A. Cervera-Lierta, T. H. Kyaw, T. Haug, S. Alperin-Lea, A. Anand, M. Degroote, H. Heimonen, J. S. Kottmann, T. Menke, W.-K. Mok, S. Sim, L.-C. Kwek, and A. Aspuru-Guzik, arXiv:2101.08448, 1 (2021), arXiv:2101.08448.
- [21] S. Endo, Z. Cai, S. C. Benjamin, and X. Yuan, arXiv:2011.01382, 1 (2020), arXiv:2011.01382.
- [22] A. Peruzzo, J. McClean, P. Shadbolt, M.-H. Yung, X.-Q. Zhou, P. J. Love, A. Aspuru-Guzik, and J. L. O’Brien, *Nature communications* **5**, 4213 (2014).
- [23] J. Romero, J. P. Olson, and A. Aspuru-Guzik, *Quantum Science and Technology* **2**, 045001 (2017), arXiv:1612.02806.
- [24] X. Wang, Z. Song, and Y. Wang, *Quantum* **5**, 483 (2021), arXiv:2006.02336.
- [25] I. Cong, S. Choi, and M. D. Lukin, *Nature Physics* **15**, 1273 (2019), arXiv:1810.03787.
- [26] W. Li and D.-L. Deng, arXiv:2108.13421 (2021), arXiv:2108.13421.
- [27] G. Li, Z. Song, and X. Wang, in *Proceedings of the AAAI Conference on Artificial Intelligence*, 35(9), 8357-8365 (2021).
- [28] M. C. Caro, H.-Y. Huang, M. Cerezo, K. Sharma, A. Sornborger, L. Cincio, and P. J. Coles, arXiv:2111.05292, 1 (2021), arXiv:2111.05292.
- [29] E. Farhi and H. Neven, arXiv:1802.06002, 1 (2018), arXiv:1802.06002.
- [30] E. Farhi, J. Goldstone, and S. Gutmann, arXiv preprint arXiv:1411.4028 (2014).
- [31] L. Zhou, S.-T. Wang, S. Choi, H. Pichler, and M. D. Lukin, *Physical Review X* **10**, 021067 (2020), arXiv:1812.01041.
- [32] M. Benedetti, E. Lloyd, S. Sack, and M. Fiorentini, *Quantum Science and Technology* **4**, 043001 (2019).
- [33] A. Kandala, A. Mezzacapo, K. Temme, M. Takita, M. Brink, J. M. Chow, and J. M. Gambetta, *Nature* **549**, 242 (2017).
- [34] M. R. Hoffmann and J. Simons, *The Journal of chemical physics* **88**, 993 (1988).
- [35] J. Lee, W. J. Huggins, M. Head-Gordon, and K. B. Whaley, *Journal of chemical theory and computation* **15**, 311 (2018).
- [36] H. R. Grimsley, S. E. Economou, E. Barnes, and N. J. Mayhall, *Nature communications* **10**, 1.
- [37] H. L. Tang, V. Shkolnikov, G. S. Barron, H. R. Grimsley, N. J. Mayhall, E. Barnes, and S. E. Economou, *PRX Quantum* **2**, 020310 (2021).
- [38] I. G. Ryabinkin, R. A. Lang, S. N. Genin, and A. F. Izmaylov, “Iterative qubit coupled cluster approach with efficient screening of generators,” (2019), arXiv:1906.11192 [quant-ph].
- [39] K. Bharti and T. Haug, *Physical Review A* **104**, L050401 (2021).
- [40] H. R. Grimsley, G. S. Barron, E. Barnes, S. E. Economou, and N. J. Mayhall, arXiv:2204.07179 (2022), arXiv:2204.07179.
- [41] T. Haug, K. Bharti, and M. S. Kim, *PRX Quantum* **2**, 1 (2021), arXiv:2102.01659.

- [42] Y. Du, Z. Tu, X. Yuan, and D. Tao, *Physical Review Letters* **128**, 80506 (2022).
- [43] Z. Holmes, K. Sharma, M. Cerezo, and P. J. Coles, *PRX Quantum* **3**, 010313 (2022).
- [44] J. R. McClean, S. Boixo, V. N. Smelyanskiy, R. Babbush, and H. Neven, *Nature communications* **9**, 1 (2018).
- [45] K. Zhang, M.-H. Hsieh, L. Liu, and D. Tao, arXiv preprint arXiv:2112.15002 (2021).
- [46] H.-K. Zhang, C. Zhu, G. Liu, and X. Wang, arXiv:2205.05056, **1** (2022), arXiv:2205.05056.
- [47] S. Sim, P. D. Johnson, and A. Aspuru-Guzik, *Advanced Quantum Technologies* **2**, 1900070 (2019).
- [48] K. Nakaji and N. Yamamoto, *Quantum* **5**, 434 (2021).
- [49] K. Sharma, M. Cerezo, L. Cincio, and P. J. Coles, *Physical Review Letters* **128**, 180505 (2022), arXiv:2005.12458.
- [50] C. Ortiz Marrero, M. Kieferová, and N. Wiebe, *PRX Quantum* **2**, 040316 (2021), arXiv:2010.15968.
- [51] E. Grant, L. Wossnig, M. Ostaszewski, and M. Benedetti, *Quantum* **3**, 214 (2019), arXiv:1903.05076.
- [52] G. Verdon, M. Broughton, J. R. McClean, K. J. Sung, R. Babbush, Z. Jiang, H. Neven, and M. Mohseni, **1** (2019), arXiv:1907.05415.
- [53] M. Cerezo, A. Sone, T. Volkoff, L. Cincio, and P. J. Coles, *Nature Communications* **12** (2021), 10.1038/s41467-021-21728-w.
- [54] M. Kieferova, O. M. Carlos, and N. Wiebe, arXiv preprint arXiv:2106.09567 (2021).
- [55] A. Pesah, M. Cerezo, S. Wang, T. Volkoff, A. T. Sornborger, and P. J. Coles, *Physical Review X* **11**, 041011 (2021), arXiv:2011.02966.
- [56] M. A. Nielsen and I. L. Chuang, *Quantum computation and quantum information* (Cambridge university press, 2010).
- [57] Y.-Y. Shi, L.-M. Duan, and G. Vidal, *Physical review a* **74**, 022320 (2006).
- [58] D. Nagaj, E. Farhi, J. Goldstone, P. Shor, and I. Sylvester, *Physical Review B* **77**, 214431 (2008).
- [59] L. Tagliacozzo, G. Evenbly, and G. Vidal, *Physical Review B* **80**, 235127 (2009).
- [60] N. Nakatani and G. K.-L. Chan, *The Journal of chemical physics* **138**, 134113 (2013).
- [61] B. G. Wybourne, (1974).
- [62] J. Biamonte, *Phys. Rev. A* **103**, L030401 (2021).
- [63] "<https://github.com/paddlepaddle/paddle>,".
- [64] Y. Ma, D. Yu, T. Wu, and H. Wang, *Frontiers of Data and Computing* **1**, 105 (2019).
- [65] J. Emerson, R. Alicki, and K. Życzkowski, *Journal of Optics B: Quantum and Semiclassical Optics* **7**, S347 (2005).
- [66] D. A. Roberts and B. Yoshida, *Journal of High Energy Physics* **2017**, 1 (2017).
- [67] E. Farhi, J. Goldstone, and S. Gutmann, arXiv:1411.4028 (2014), arXiv:1411.4028.
- [68] K. Wang, Z. Song, X. Zhao, Z. Wang, and X. Wang, *npj Quantum Information* **8**, 1 (2022).
- [69] H. L. Tang, V. Shkolnikov, G. S. Barron, H. R. Grimsley, N. J. Mayhall, E. Barnes, and S. E. Economou, *PRX Quantum* **2**, 020310 (2021).
- [70] A. Skolik, J. R. McClean, M. Mohseni, P. van der Smagt, and M. Leib, *Quantum Machine Intelligence* **3**, 1 (2021).
- [71] T. Volkoff and P. J. Coles, *Quantum Science and Technology* **6**, 025008 (2021), arXiv:2005.12200.
- [72] G. Verdon, M. Broughton, J. R. McClean, K. J. Sung, R. Babbush, Z. Jiang, H. Neven, and M. Mohseni, arXiv preprint arXiv:1907.05415 (2019).
- [73] M. Wilson, R. Stromswold, F. Wudarski, S. Hadfield, N. M. Tubman, and E. G. Rieffel, *Quantum Machine Intelligence* **3**, 1 (2021).
- [74] T. Stollenwerk and S. Hadfield, arXiv preprint arXiv:2204.01307 (2022).
- [75] C. Chen, Z. He, L. Li, S. Zheng, and H. Situ, arXiv preprint arXiv:2106.06248 (2021).
- [76] H. Zheng, Z. Li, J. Liu, S. Strelchuk, and R. Kondor, arXiv preprint arXiv:2112.07611 (2021).
- [77] J. J. Meyer, M. Mularski, E. Gil-Fuster, A. A. Mele, F. Arzani, A. Wilms, and J. Eisert, arXiv preprint arXiv:2205.06217 (2022).
- [78] M. Larocca, F. Sauvage, F. M. Sbahi, G. Verdon, P. J. Coles, and M. Cerezo, arXiv preprint arXiv:2205.02261 (2022).
- [79] C. Dankert, R. Cleve, J. Emerson, and E. Livine, *Physical Review A* **80**, 012304 (2009).
- [80] W. Feit, *The representation theory of finite groups* (Elsevier, 1982).



# Supplemental Material for Mitigating barren plateaus of variational quantum eigensolvers

## I. PRELIMINARIES

Here we present some supplemental lemmas and define some notations to be used throughout the proof. We write a target quantum state, which is a pure state to be approximated by a PQC, as  $|\phi\rangle$  and let the actual circuit output be  $|\psi(\boldsymbol{\theta})\rangle$ . We may simply write  $|\psi\rangle$  if the circuit parameters  $\boldsymbol{\theta}$  are unimportant in the context. Moreover, let  $F(|\phi\rangle, |\psi\rangle) = |\langle\psi|\phi\rangle|^2$  be fidelity. Unless otherwise specified,  $\{|k\rangle\}_{k=0}^{2^N-1}$  are the  $N$ -qubit computational bases. We denote  $\widetilde{\text{CNOT}} \equiv \prod_{i=0}^{N-i} \text{CNOT}(i, N+i)$  which is a composition of  $N$  CNOTs controlled and targeted on the pair  $(i, N+i)$  for all  $i = 0, \dots, N-1$ . Let  $\bar{i}$  be a vector for the binary expansion of  $i$ , and therefore  $\bar{i}_j$ , where  $0 \leq j < \lceil \log i \rceil$ , is the  $j$ -th leading digit of the expansion.

### A. $t$ -design and integration over the unitary group

We firstly recall the definition of a  $t$ -design. Assume  $\mathcal{U} = \{U_k\}_{k=1}^K$  is a finite of unitary operator on  $\mathbb{C}^D$ , and  $P_{t,t}(U)$  is a polynomial of degree at most  $t$  in the matrix elements of  $U$  and at most  $t$  in those of  $U^\dagger$ . Then, we define that  $\mathcal{U}$  is a  $t$ -design if for every polynomial  $P_{t,t}(U)$  we have

$$\frac{1}{K} \sum_{k=1}^K P_{t,t}(U_k) = \int P_{t,t}(U) d\eta(U), \quad (\text{A1})$$

where the integrals with respect to the Haar measure over the unitary group. Particularly, when  $t = 2$ , the definition is equivalent to the following definition [79].

**Definition S1**  $\{U_k\}_{k=1}^K$  forms a unitary 2-design if and only if for any linear operators  $C, D, \rho \in L(\mathbb{C}^D)$ , we have

$$\frac{1}{K} \sum_{k=1}^K U_k^\dagger C U_k \rho U_k^\dagger D U_k = \int_{\mathcal{U}(d)} U^\dagger C U \rho U^\dagger D U d\eta(U). \quad (\text{A2})$$

Based on this definition, we can know whether a unitary group is a 2-design by comparing the both sides of Eq. (A2). Fortunately, according to the Schur's lemma [80], the RHS of Eq. (A3) has a closed form which is shown in lemma S1. The proof of lemma S1 can be seen in [65].

**Lemma S1** Let  $\{U_k\}_{k=1}^K$  forms a unitary  $t$ -design with  $t \geq 2$ , for any linear operators  $C, D, \rho \in L(\mathbb{C}^D)$ . We have

$$\int_{\mathcal{U}(d)} U^\dagger C U \rho U^\dagger D U d\eta(U) = \frac{\text{Tr}[CD] \text{Tr}[\rho]}{d} \frac{I}{d} + \left( \frac{d \text{Tr}[C] \text{Tr}[D] - \text{Tr}[CD]}{d(d^2 - 1)} \right) (\rho - \text{Tr}[\rho] \frac{I}{d}). \quad (\text{A3})$$

Furthermore, we present the following lemma so that we can solve the problem with bipartite system.

**Lemma 2** For any bipartite state  $\rho_{AB}$  ( $d_A = d_B = d$ ), and arbitrary linear operators  $C, D \in L(\mathbb{C}^{d^2})$ , we have

$$\int_{\mathcal{U}(d) \otimes \mathcal{U}(d)} d\eta(U) U^\dagger C U \rho U^\dagger D U = t_0 \rho + t_1 \frac{\rho_A \otimes I_B}{d} + t_2 \frac{I_A \otimes \rho_B}{d} + t_3 I_{AB} \text{Tr}(\rho_{AB}), \quad (\text{A4})$$

where  $\rho_A = \text{Tr}_B[\rho_{AB}]$ ,  $\rho_B = \text{Tr}_A[\rho_{AB}]$ , and  $\{t_j\}_{j=0}^3$  can be computed from the following linear system of equations

$$\text{Tr}(CD) = t_0 d^2 + t_1 d^2 + t_2 d^2 + t_3 d^4, \quad (\text{A5})$$

$$\text{Tr}(C_A D_A) = t_0 d^3 + t_1 d + t_2 d^3 + t_3 d^3, \quad (\text{A6})$$

$$\text{Tr}(C_B D_B) = t_0 d^3 + t_1 d^3 + t_2 d + t_3 d^3, \quad (\text{A7})$$

$$\text{Tr}(C) \text{Tr}(D) = t_0 d^4 + t_1 d^2 + t_2 d^2 + t_3 d^2, \quad (\text{A8})$$

that is,

$$\begin{bmatrix} t_0 \\ t_1 \\ t_2 \\ t_3 \end{bmatrix} = \frac{1}{(d^2 - 1)^2} \begin{bmatrix} \frac{\text{Tr}[CD]}{d^2} - \frac{\text{Tr}[C_A D_A]}{d} - \frac{\text{Tr}[C_B D_B]}{d} + \text{Tr}[C] \text{Tr}[D] \\ -\text{Tr}[CD] + \frac{\text{Tr}[C_A D_A]}{d} + d \text{Tr}[C_B D_B] - \text{Tr}[C] \text{Tr}[D] \\ -\text{Tr}[CD] + d \text{Tr}[C_A D_A] + \frac{\text{Tr}[C_B D_B]}{d} - \text{Tr}[C] \text{Tr}[D] \\ \text{Tr}[CD] - \frac{\text{Tr}[C_A D_A]}{d} - \frac{\text{Tr}[C_B D_B]}{d} + \frac{\text{Tr}[C] \text{Tr}[D]}{d^2} \end{bmatrix}. \quad (\text{A9})$$

**Proof** Similar to the proof of Lemma S1, Schur's lemma implies that the LHS of Eq. (4) has an explicitly expression, which is denoted as follows:

$$\int_{\mathcal{U}(d) \otimes \mathcal{U}(d)} d\eta(U) U^\dagger C U \rho U^\dagger D U = t_0 \rho + t_1 \frac{\rho_A \otimes I_B}{d} + t_2 \frac{I_A \otimes \rho_B}{d} + t_3 I_{AB} \text{Tr}(\rho_{AB}). \quad (\text{A10})$$

For simplicity, we define the following two functions:

$$f^{(1)}(\rho) \equiv t_0 \rho + t_1 \rho_A \otimes I_B / d + t_2 I_A \otimes \rho_B / d + t_3 I_{AB} \text{Tr}(\rho_{AB}), \quad (\text{A11})$$

$$f^{(2)}(\rho) \equiv \int_{\mathcal{U}(d) \otimes \mathcal{U}(d)} d\eta(U) U^\dagger C U \rho U^\dagger D U, \quad (\text{A12})$$

where  $f^{(1)} = f^{(2)}$ .

Then we only need to consider the coefficients  $t_0, t_1, t_2, t_3$ . To calculate the coefficients, we defined the following four operators:

$$T_1(f) \equiv \sum_{i,j} \langle ij | f(I) | ij \rangle, \quad (\text{A13})$$

$$T_2(f) \equiv \sum_{i,j,k} \langle ik | f(|i\rangle\langle j|_A \otimes I_B) | jk \rangle, \quad (\text{A14})$$

$$T_3(f) \equiv \sum_{i,k,l} \langle ik | f(I_A \otimes |k\rangle\langle l|_B) | il \rangle, \quad (\text{A15})$$

$$T_4(f) \equiv \sum_{i,j,k,l} \langle ij | f(|ij\rangle\langle kl|) | kl \rangle. \quad (\text{A16})$$

For Eq. (A5), we have

$$\begin{aligned} T_1(f^{(1)}) &= t_0 \sum_{i,j} \langle ij | I | ij \rangle + t_1 \sum_{i,j} \langle ij | I_A \otimes I_B | ij \rangle + t_2 \sum_{i,j} \langle ij | I_A \otimes I_B | ij \rangle + t_3 d^4 \\ &= t_0 d^2 + t_1 d^2 + t_2 d^2 + t_3 d^4, \end{aligned}$$

$$\begin{aligned} T_1(f^{(2)}) &= \sum_{i,j} \langle ij | \int_{\mathcal{U}(d) \otimes \mathcal{U}(d)} d\eta(U) U^\dagger C U I U^\dagger D U | ij \rangle \\ &= \text{Tr}(CD). \end{aligned}$$

Since  $T_1(f^{(1)}) = T_1(f^{(2)})$ , then  $\text{Tr}(CD) = t_0 d^2 + t_1 d^2 + t_2 d^2 + t_3 d^4$ .

For Eq. (A7), we have

$$\begin{aligned} T_2(f^{(1)}) &= t_0 \sum_{i,j,k} \langle ik | |i\rangle\langle j| \otimes I_B | jk \rangle + t_1 \sum_{i,j,k} \langle ik | |i\rangle\langle j| \otimes I_B | jk \rangle \\ &\quad + \frac{t_2}{d} \sum_{i,j,k} \langle ik | I_A \otimes \text{Tr}[|i\rangle\langle j|] I_B | jk \rangle + t_3 \sum_{i,j,k} \langle ik | I_{AB} \text{Tr}[|i\rangle\langle j| \otimes I_B] | jk \rangle \\ &= t_0 d^3 + t_1 d^3 + t_2 d + t_3 d^3, \end{aligned}$$

$$\begin{aligned} T_2(f^{(2)}) &= \sum_{i,j,k} \langle ik | \int_{\mathcal{U}(d) \otimes \mathcal{U}(d)} d\eta(U) U^\dagger C U (|i\rangle\langle j|_A \otimes I_B) U^\dagger D U | jk \rangle \\ &= \sum_{i,j,k} \int_{\mathcal{U}(d) \otimes \mathcal{U}(d)} d\eta(U) \langle ik | U^\dagger C U (|i\rangle\langle j|_A \otimes I_B) U^\dagger D U | jk \rangle \\ &= \text{Tr}(C_B D_B). \end{aligned}$$

Since  $T_2(f^{(1)}) = T_2(f^{(2)})$ , then  $\text{Tr}(C_B D_B) = t_0 d^3 + t_1 d^3 + t_2 d + t_3 d^3$ .

Similarly, we have

$$T_3(f^{(1)}) = t_0 d^3 + t_1 d + t_2 d^3 + t_3 d^3,$$

$$\begin{aligned}
T_3(f^{(2)}) &= \text{Tr}(C_A D_A), \\
T_4(f^{(1)}) &= t_0 d^4 + t_1 d^2 + t_2 d^2 + t_3 d^2, \\
T_4(f^{(2)}) &= \text{Tr}(C) \text{Tr}(D).
\end{aligned}$$

Since

$$\begin{aligned}
T_3(f^{(1)}) &= T_3(f^{(2)}), \\
T_4(f^{(1)}) &= T_4(f^{(2)}),
\end{aligned}$$

then

$$\begin{aligned}
\text{Tr}(C_A D_A) &= t_0 d^3 + t_1 d + t_2 d^3 + t_3 d^3, \\
\text{Tr}(C) \text{Tr}(D) &= t_0 d^4 + t_1 d^2 + t_2 d^2 + t_3 d^2.
\end{aligned}$$

Up to now, we have proved Eq. (A5) to Eq. (A8).

Let

$$R = \begin{pmatrix} d^2 & d^2 & d^2 & d^4 \\ d^3 & d^1 & d^3 & d^3 \\ d^3 & d^3 & d^1 & d^3 \\ d^4 & d^2 & d^2 & d^2 \end{pmatrix}. \quad (\text{A17})$$

Then

$$R^{-1} = \frac{1}{(d^2 - 1)^2} \begin{pmatrix} \frac{1}{d^2} & -\frac{1}{d} & -\frac{1}{d} & 1 \\ -1 & \frac{1}{d} & d & -1 \\ -1 & d & \frac{1}{d} & -1 \\ 1 & -\frac{1}{d} & -\frac{1}{d} & \frac{1}{d^2} \end{pmatrix}. \quad (\text{A18})$$

Hence, we have

$$\begin{bmatrix} t_0 \\ t_1 \\ t_2 \\ t_3 \end{bmatrix} = R^{-1} \begin{bmatrix} \text{Tr}(CD) \\ \text{Tr}(C_A D_A) \\ \text{Tr}(C_B D_B) \\ \text{Tr}(C) \text{Tr}(D) \end{bmatrix} = \frac{1}{(d^2 - 1)^2} \begin{bmatrix} \frac{\text{Tr}[CD]}{d^2} - \frac{\text{Tr}[C_A D_A]}{d} - \frac{\text{Tr}[C_B D_B]}{d} + \text{Tr}[C] \text{Tr}[D] \\ -\text{Tr}[CD] + \frac{\text{Tr}[C_A D_A]}{d} + d \text{Tr}[C_B D_B] - \text{Tr}[C] \text{Tr}[D] \\ -\text{Tr}[CD] + d \text{Tr}[C_A D_A] + \frac{\text{Tr}[C_B D_B]}{d} - \text{Tr}[C] \text{Tr}[D] \\ \text{Tr}[CD] - \frac{\text{Tr}[C_A D_A]}{d} - \frac{\text{Tr}[C_B D_B]}{d} + \frac{\text{Tr}[C] \text{Tr}[D]}{d^2} \end{bmatrix}, \quad (\text{A19})$$

$$\begin{bmatrix} t_0 \\ t_1 \\ t_2 \\ t_3 \end{bmatrix} = \frac{1}{(d^2 - 1)^2} \begin{bmatrix} \frac{\text{Tr}[CD]}{d^2} - \frac{\text{Tr}[C_A D_A]}{d} - \frac{\text{Tr}[C_B D_B]}{d} + \text{Tr}[C] \text{Tr}[D] \\ -\text{Tr}[CD] + \frac{\text{Tr}[C_A D_A]}{d} + d \text{Tr}[C_B D_B] - \text{Tr}[C] \text{Tr}[D] \\ -\text{Tr}[CD] + d \text{Tr}[C_A D_A] + \frac{\text{Tr}[C_B D_B]}{d} - \text{Tr}[C] \text{Tr}[D] \\ \text{Tr}[CD] - \frac{\text{Tr}[C_A D_A]}{d} - \frac{\text{Tr}[C_B D_B]}{d} + \frac{\text{Tr}[C] \text{Tr}[D]}{d^2} \end{bmatrix}. \quad (\text{A20})$$

■

## II. PROOF OF THEOREM 1

**Lemma S2**  $\widehat{\text{CNOT}} = \sum_{i=0}^{2^n-1} |i\rangle\langle i|_A \otimes V_{B_i}$ , where  $A, B$  are subsystems and  $V_{B_i} = \bigotimes_{j=0}^{n-1} X_j^{i_j}$ ,  $i_j \in \{0, 1\}$ , that is the operator on the subsystem  $B$  that represents the binary bit of  $i$  is 1 acting on pauli  $X$ , and 0 acting on  $I$ . Then  $V_{B_i}$  has the following properties:

1.  $[V_{B_i}, V_{B_j}] = 0$ ;
2.  $V_{B_i} = V_{B_i}^\dagger$ ;
3.  $\langle 0 |^{\otimes n} V_{B_i} V_{B_j} | 0 \rangle^{\otimes n} = \delta_{ij}$ ,

where  $\delta_{ij}$  is Kronecker delta.

**Theorem 1** SEA with  $U_i (i = 1, 2, 3)$  being local 2-design and  $\widetilde{\text{CNOT}}$  as entangling layer does not form a 2-design on the global system.

**Proof** Without losing generality, we only consider the SEA with  $2n$  qubits in this proof. Lemma S1 says that if an ansatz forms a 2-design, the Eq. (A3) should hold for any linear operators  $C, D, \rho \in L(\mathbb{C}^{d^2})$ . Assuming  $d = 2^n, C_0 = D_0 = \rho = |0\rangle\langle 0|^{\otimes 2n}$ , then if SEA forms a 2-design, we have

$$\int_{U(\theta)} \langle 0|^{\otimes 2n} U^\dagger C_0 U \rho U^\dagger D_0 U |0\rangle^{\otimes 2n} d\eta(U) \quad (\text{A21})$$

$$= \int_{\mathcal{U}(d^2)} \langle 0|^{\otimes 2n} U^\dagger C_0 U \rho U^\dagger D_0 U |0\rangle^{\otimes 2n} d\eta(U) \quad (\text{A22})$$

$$= \frac{2}{d^2(d^2 + 1)}, \quad (\text{A23})$$

where  $U(\theta)$  denotes the subset of unitary group generated by SEA, and  $d\eta(U)$  denotes the Haar measure.

In the following steps, we will explicitly calculate the Eq. (A21) and prove that it cannot be  $\frac{2}{d^2(d^2+1)}$ .

For the SEA with  $U_i (i = 1, 2, 3)$  being local 2-design and  $\widetilde{\text{CNOT}} = V = \sum_{i=0}^{2^n-1} |i\rangle\langle i|_A \otimes V_{B_i}$ , the unitary of this ansatz is

$$U = \sum_{i=0}^{2^n-1} (U_2 \otimes U_3) \cdot |i\rangle\langle i| \otimes V_{B_i} \cdot (U_1 \otimes I_B). \quad (\text{A24})$$

Therefore,

$$\begin{aligned} U|0\rangle^{\otimes 2n} &= \sum_{i=0}^{2^n-1} (U_2 \otimes U_3) \cdot |i\rangle\langle i| \otimes V_{B_i} \cdot (U_1 \otimes I_B) |0\rangle^{\otimes 2n}, \\ \langle 0|^{\otimes 2n} U^\dagger &= \sum_{i=0}^{2^n-1} \langle 0|^{\otimes 2n} (U_1^\dagger \otimes I_B) \cdot |i\rangle\langle i| \otimes V_{B_i} \cdot (U_2^\dagger \otimes U_3^\dagger). \end{aligned}$$

Then

$$\begin{aligned} &\langle 0|^{\otimes 2n} U^\dagger C_0 U \rho U^\dagger D_0 U |0\rangle^{\otimes 2n} \\ &= \langle 0|^{\otimes 2n} U^\dagger (|0\rangle\langle 0|)^{\otimes 2n} U (|0\rangle\langle 0|)^{\otimes 2n} U^\dagger (|0\rangle\langle 0|)^{\otimes 2n} U |0\rangle^{\otimes 2n} \\ &= \langle 0|^{\otimes 2n} (U_1^\dagger \otimes I_B) \cdot V^\dagger \cdot (U_2^\dagger \otimes U_3^\dagger) (|0\rangle\langle 0|)^{\otimes 2n} (U_2 \otimes U_3) \cdot V \cdot (U_1 \otimes I_B) (|0\rangle\langle 0|)^{\otimes 2n} (U_1^\dagger \otimes I_B) \cdot V^\dagger \\ &\quad \cdot (U_2^\dagger \otimes U_3^\dagger) (|0\rangle\langle 0|)^{\otimes 2n} (U_2 \otimes U_3) \cdot V \cdot (U_1 \otimes I_B) |0\rangle^{\otimes 2n} \\ &:= \langle 0|^{\otimes 2n} (U_1^\dagger \otimes I_B) \cdot V^\dagger \cdot (U_2^\dagger \otimes U_3^\dagger) \cdot C_0 \cdot (U_2 \otimes U_3) \cdot \rho_1 \cdot (U_2^\dagger \otimes U_3^\dagger) \cdot D_0 \cdot (U_2 \otimes U_3) \cdot V \\ &\quad \cdot (U_1 \otimes I_B) |0\rangle^{\otimes 2n}, \end{aligned}$$

where

$$\begin{aligned} V &= \sum_{i=0}^{2^n-1} |i\rangle\langle i|_A \otimes V_{B_i}, \\ \rho_1 &= V \cdot (U_1 \otimes I_B) (|0\rangle\langle 0|)^{\otimes 2n} (U_1^\dagger \otimes I_B) \cdot V^\dagger. \end{aligned}$$

Therefore, we have

$$\begin{aligned} \rho_1^A &= \text{Tr}_B[\rho_1] \\ &= \sum_{k=0}^{d-1} I_A \otimes \langle k|_B \cdot V \cdot (U_1 \otimes I_B) (|0\rangle\langle 0|)^{\otimes 2n} \cdot (U_1^\dagger \otimes I_B) \cdot V^\dagger \cdot I_A \otimes |k\rangle_B \\ &= \sum_{k=0}^{d-1} I_A \otimes \langle k|_B \cdot \left( \sum_{i=0}^{d-1} |i\rangle\langle i|_A \otimes V_{B_i} \right) \cdot (U_1 \otimes I_B) (|0\rangle\langle 0|)^{\otimes 2n} \cdot (U_1^\dagger \otimes I_B) \cdot \left( \sum_{j=0}^{d-1} |j\rangle\langle j|_A \otimes V_{B_j}^\dagger \right) \cdot I_A \otimes |k\rangle_B \end{aligned}$$

$$\begin{aligned}
&= \sum_{i,j,k=0}^{d-1} I_A \otimes \langle k|_B \cdot (|i\rangle\langle i|_A \otimes V_{B_i}) \cdot (U_1 \otimes I_B) (|0\rangle\langle 0|)^{\otimes 2n} \cdot (U_1^\dagger \otimes I_B) \cdot (|j\rangle\langle j|_A \otimes V_{B_j}^\dagger) \cdot I_A \otimes |k\rangle_B \\
&= \sum_{i,j,k=0}^{d-1} |i\rangle\langle i|_A U_1 (|0\rangle\langle 0|)^{\otimes n} U_1^\dagger |j\rangle\langle j|_A \otimes \langle k|_B V_{B_i} (|0\rangle\langle 0|)^{\otimes n} V_{B_j}^\dagger |k\rangle_B \\
&= \sum_{i,j=0}^{d-1} |i\rangle\langle i|_A U_1 (|0\rangle\langle 0|)^{\otimes n} U_1^\dagger |j\rangle\langle j|_A \left( \sum_{k=0}^{d-1} \langle k|_B V_{B_i} (|0\rangle\langle 0|)^{\otimes n} V_{B_j}^\dagger |k\rangle_B \right) \\
&= \sum_{i,j=0}^{d-1} |i\rangle\langle i|_A U_1 (|0\rangle\langle 0|)^{\otimes n} U_1^\dagger |j\rangle\langle j|_A \text{Tr}(V_{B_i} (|0\rangle\langle 0|)^{\otimes n} V_{B_j}^\dagger) \\
&= \sum_{i,j=0}^{d-1} |i\rangle\langle i|_A U_1 (|0\rangle\langle 0|)^{\otimes n} U_1^\dagger |j\rangle\langle j|_A \text{Tr}(\langle 0|^{\otimes n} V_{B_i} V_{B_j}^\dagger |0\rangle^{\otimes n}) \\
&= \sum_{i=0}^{d-1} |i\rangle\langle i| U_1 |0\rangle\langle 0|^{\otimes n} U_1^\dagger |i\rangle\langle i|, \quad (\text{due to lemma S2}) \\
\rho_1^B &= \text{Tr}_A[\rho_1] \\
&= \sum_{k=0}^{d-1} \langle k|_A \otimes I_B \cdot V \cdot (U_1 \otimes I_B) (|0\rangle\langle 0|)^{\otimes 2n} \cdot (U_1^\dagger \otimes I_B) \cdot V^\dagger \cdot |k\rangle_A \otimes I_B \\
&= \sum_{k=0}^{d-1} \langle k|_A \otimes I_B \cdot \left( \sum_{i=0}^{d-1} |i\rangle\langle i|_A \otimes V_{B_i} \right) \cdot (U_1 \otimes I_B) (|0\rangle\langle 0|)^{\otimes 2n} \cdot (U_1^\dagger \otimes I_B) \cdot \left( \sum_{j=0}^{d-1} |j\rangle\langle j|_A \otimes V_{B_j}^\dagger \right) \cdot |k\rangle_A \otimes I_B \\
&= \sum_{i,j,k=0}^{d-1} \langle k|_A |i\rangle\langle i|_A U_1 (|0\rangle\langle 0|)^{\otimes n} U_1^\dagger |j\rangle\langle j|_A |k\rangle_A \cdot V_{B_i} (|0\rangle\langle 0|)^{\otimes n} V_{B_j} \\
&= \sum_{k=0}^{d-1} \langle k| U_1 |0\rangle\langle 0|^{\otimes n} U_1^\dagger |k\rangle \cdot V_{B_k} |0\rangle\langle 0|^{\otimes n} V_{B_k}.
\end{aligned}$$

Then combining lemma S1 and lemma 2, we have

$$\begin{aligned}
&\int_{U(\theta)} \langle 0|^{\otimes 2n} U^\dagger C_0 U \rho U^\dagger D_0 U |0\rangle^{\otimes 2n} d\eta(U) \\
&= \int_{U(\theta)} \langle 0|^{\otimes 2n} (U_1^\dagger \otimes I_B) \cdot V^\dagger \cdot (U_2^\dagger \otimes U_3^\dagger) \cdot C_0 \cdot (U_2 \otimes U_3) \cdot \rho_1 \cdot (U_2^\dagger \otimes U_3^\dagger) \cdot D_0 \cdot (U_2 \otimes U_3) \cdot V \\
&\quad \cdot (U_1 \otimes I_B) |0\rangle^{\otimes 2n} \tag{A25}
\end{aligned}$$

$$\begin{aligned}
&= \int_{\mathcal{U}_1(d)} \langle 0|^{\otimes 2n} (U_1^\dagger \otimes I_B) \cdot V^\dagger \cdot (t_0 \rho_1 + t_1 \frac{\rho_1^A \otimes I_B}{d} + t_2 \frac{I_A \otimes \rho_1^B}{d} + t_3 I_{AB} \text{Tr}(\rho_1)) \cdot V \\
&\quad \cdot (U_1 \otimes I_B) |0\rangle^{\otimes 2n} d\eta(U) \\
&:= M_0 + M_1 + M_2 + M_3, \tag{A26}
\end{aligned}$$

where

$$\begin{aligned}
M_0 &= t_0 \int_{\mathcal{U}_1(d)} \langle 0|^{\otimes 2n} (U_1^\dagger \otimes I_B) \cdot V^\dagger \cdot \rho_1 \cdot V \cdot (U_1 \otimes I_B) |0\rangle^{\otimes 2n} d\eta(U) \\
&= t_0, \\
M_1 &= \frac{t_1}{d} \int_{\mathcal{U}_1(d)} \langle 0|^{\otimes 2n} (U_1^\dagger \otimes I_B) \cdot V^\dagger \cdot \rho_1^A \otimes I_B \cdot V \cdot (U_1 \otimes I_B) |0\rangle^{\otimes 2n} d\eta(U), \\
M_2 &= \frac{t_2}{d} \int_{\mathcal{U}_1(d)} \langle 0|^{\otimes 2n} (U_1^\dagger \otimes I_B) \cdot V^\dagger \cdot I_A \otimes \rho_1^B \cdot V \cdot (U_1 \otimes I_B) |0\rangle^{\otimes 2n} d\eta(U), \\
M_3 &= t_3 \int_{\mathcal{U}_1(d)} \langle 0|^{\otimes 2n} (U_1^\dagger \otimes I_B) \cdot V^\dagger \cdot I_{AB} \text{Tr}(\rho_1) \cdot V \cdot (U_1 \otimes I_B) |0\rangle^{\otimes 2n} d\eta(U)
\end{aligned}$$

$$\begin{aligned}
&= t_3, \\
t_0 = t_3 &= \frac{1}{d^2(d+1)^2}, \\
t_1 = t_2 &= \frac{1}{d(d+1)^2}.
\end{aligned}$$

Now the problem is how do we calculate  $M_1$  and  $M_2$ . Combine with  $V = \sum_{i=0}^{d-1} |i\rangle\langle i|_A \otimes V_{B_i}$ , there has

$$\begin{aligned}
M_1 &= \frac{t_1}{d} \int_{\mathcal{U}_1(d)} \langle 0|^{\otimes 2n} (U_1^\dagger \otimes I_B) \cdot V^\dagger \cdot \rho_1^A \otimes I_B \cdot V \cdot (U_1 \otimes I_B) |0\rangle^{\otimes 2n} d\eta(U) \\
&= \frac{t_1}{d} \int_{\mathcal{U}_1(d)} \langle 0|^{\otimes 2n} (U_1^\dagger \otimes I_B) \left( \sum_{i=0}^{d-1} |i\rangle\langle i| \otimes V_{B_i}^\dagger \right) \cdot \left( \sum_{k=0}^{d-1} |k\rangle\langle k| U_1 |0\rangle\langle 0|^{\otimes n} U_1^\dagger |k\rangle\langle k| \otimes I_B \right) \\
&\quad \cdot \left( \sum_{j=0}^{d-1} |j\rangle\langle j| \otimes V_{B_j} \right) (U_1 \otimes I_B) |0\rangle^{\otimes 2n} d\eta(U) \\
&= \frac{t_1}{d} \sum_{i=0}^{d-1} \int_{\mathcal{U}_1(d)} \langle 0|^{\otimes n} U_1^\dagger |i\rangle\langle i| U_1 (|0\rangle\langle 0|)^{\otimes n} U_1^\dagger |i\rangle\langle i| U_1 |0\rangle^{\otimes n} \cdot (\langle 0|0\rangle)^{\otimes n} d\eta(U) \\
&= \frac{2t_1}{d(d+1)}, \tag{A27}
\end{aligned}$$

$$\begin{aligned}
M_2 &= \frac{t_2}{d} \int_{\mathcal{U}_1(d)} \langle 0|^{\otimes 2n} (U_1^\dagger \otimes I_B) \cdot V^\dagger \cdot I_A \otimes \rho_1^B \cdot V \cdot (U_1 \otimes I_B) |0\rangle^{\otimes 2n} d\eta(U) \\
&= \frac{t_2}{d} \int_{\mathcal{U}_1(d)} \langle 0|^{\otimes 2n} (U_1^\dagger \otimes I_B) \left( \sum_{i=0}^{d-1} |i\rangle\langle i| \otimes V_{B_i}^\dagger \right) \cdot \left( I_A \otimes \sum_{k=0}^{d-1} |k\rangle\langle k| U_1 |0\rangle\langle 0|^{\otimes n} U_1^\dagger |k\rangle\langle k| V_{B_k} |0\rangle\langle 0|^{\otimes n} V_{B_k} \right) \\
&\quad \cdot \left( \sum_{j=0}^{d-1} |j\rangle\langle j| \otimes V_{B_j} \right) (U_1 \otimes I_B) |0\rangle^{\otimes 2n} d\eta(U) \\
&= \frac{t_2}{d} \sum_{i=0}^{d-1} \int_{\mathcal{U}_1(d)} \langle 0|^{\otimes n} U_1^\dagger |i\rangle\langle i| U_1 (|0\rangle\langle 0|)^{\otimes n} U_1^\dagger |i\rangle\langle i| U_1 |0\rangle^{\otimes n} \cdot (\langle 0|0\rangle)^{\otimes n} d\eta(U) \\
&= \frac{2t_2}{d(d+1)}. \tag{A28}
\end{aligned}$$

Therefore,

$$\begin{aligned}
\text{Eq. (A26)} &= M_0 + M_1 + M_2 + M_3 \\
&= \frac{2d+6}{d^2(d+1)^3} \\
&\neq \frac{2}{d^2(d^2+1)} \quad (n \geq 1, d = 2^n > 1) \\
&= \text{Eq. (A23)}. \tag{A29}
\end{aligned}$$

Thus, SEA with  $U_i (i = 1, 2, 3)$  being local 2-design ansatzes and  $\widetilde{\text{CNOT}}$  is not a unitary 2-design.  $\blacksquare$

### III. PROOF OF PROPERTY 1 AND PROPERTY 2

**Property 1** *If  $U_1$  can generate an arbitrary  $N$ -qubit pure state, then given any  $2N$ -qubit pure state  $|\phi\rangle$ , a  $2N$ -qubit SEA can generate  $|\phi\rangle$  with a certain set of parameters  $\hat{\theta} = \{\hat{\theta}_1, \hat{\theta}_2, \hat{\theta}_3\}$ , that is,*

$$S(\hat{\theta})|0\rangle^{\otimes 2N} = |\phi\rangle. \tag{A30}$$

**Proof**

Beginning with Schmidt decomposition, we can write the target state  $|\phi\rangle$  as

$$|\phi\rangle = (\hat{U}_2 \otimes \hat{U}_3) \sum_{k=0}^{2^N-1} \lambda_k |k\rangle_A |k\rangle_B,$$

where  $A$  and  $B$  are two  $N$ -qubit subsystems,  $\hat{U}_2$  and  $\hat{U}_3$  are two unitary operators acting on these two subsystems,  $\{|k\rangle\}_{k=0}^{2^N-1}$  are the  $N$ -qubit computational bases, and  $\{\lambda_k\}_{k=0}^{2^N-1}$  are Schmidt coefficients.

Because  $U_1(\boldsymbol{\theta}_1)$  can generate an arbitrary  $N$ -qubit pure state, and  $U_2(\boldsymbol{\theta}_2), U_3(\boldsymbol{\theta}_3)$  are universal, we can choose a certain set of parameters  $\hat{\boldsymbol{\theta}} = \{\hat{\boldsymbol{\theta}}_1, \hat{\boldsymbol{\theta}}_2, \hat{\boldsymbol{\theta}}_3\}$  such that

$$U_1(\hat{\boldsymbol{\theta}}_1)|0\rangle^{\otimes N} = \sum_{k=0}^{2^N-1} \lambda_k |k\rangle, \quad (\text{A31})$$

$$U_2(\hat{\boldsymbol{\theta}}_2) = \hat{U}_2, \quad (\text{A32})$$

$$U_3(\hat{\boldsymbol{\theta}}_3) = \hat{U}_3. \quad (\text{A33})$$

Combining with  $V$ , which is a composition of  $N$  CNOTs controlled and targeted on the qubit-pairs  $\{(i, N+1)\}_{i=0}^{N-1}$ , there has

$$\begin{aligned} V(U_1(\boldsymbol{\theta}_1) \otimes I)|0\rangle_A^{\otimes N}|0\rangle_B^{\otimes N} &= \sum_{k=0}^{2^N-1} \lambda_k V|k\rangle_A|0\rangle_B^{\otimes N} \\ &= \sum_{k=0}^{2^N-1} \lambda_k |k\rangle_A |k\rangle_B. \end{aligned}$$

Therefore, we have

$$\begin{aligned} S(\hat{\boldsymbol{\theta}})|0\rangle^{\otimes 2N} &= (U_2(\hat{\boldsymbol{\theta}}_2) \otimes U_3(\hat{\boldsymbol{\theta}}_3))V(U_1(\hat{\boldsymbol{\theta}}_1) \otimes I)|0\rangle^{\otimes N}|0\rangle^{\otimes N} \\ &= (\hat{U}_2 \otimes \hat{U}_3) \sum_{k=0}^{2^N-1} \lambda_k |k\rangle_A |k\rangle_B. \\ &= |\phi\rangle. \end{aligned}$$

■

**Lemma S3** For any descending sequence  $\{x_i\}_{i=1}^n$  ( $x_i \geq x_{i+1}$ ), and any  $n \geq N \geq M \geq 1$  ( $n, N, M \in \mathbb{Z}$ ), the following is true:

$$\frac{1}{M} \sum_{i=1}^M x_i \geq \frac{1}{N} \sum_{i=1}^N x_i.$$

**Proof** Because  $N \geq M \geq 1$  and  $x_i \geq x_{i+1}$ , we have the following formula:

$$\begin{aligned} &\frac{1}{M} \sum_{i=1}^M x_i - \frac{1}{N} \sum_{i=1}^N x_i \\ &= \frac{1}{M} \sum_{i=1}^M x_i - \left( \frac{1}{N} \sum_{i=1}^M x_i + \frac{1}{N} \sum_{i=M+1}^N x_i \right) \\ &= \left( \frac{1}{M} - \frac{1}{N} \right) \sum_{i=1}^M x_i - \frac{1}{N} \sum_{i=M+1}^N x_i \\ &= \frac{1}{N} \left( \frac{N-M}{M} \sum_{i=1}^M x_i - \sum_{i=M+1}^N x_i \right) \\ &= \frac{N-M}{N} \left( \frac{1}{M} \sum_{i=1}^M x_i - \frac{1}{N-M} \sum_{i=M+1}^N x_i \right) \end{aligned}$$

$$\begin{aligned}
&\geq \frac{N-M}{N} \left( \frac{1}{M} \sum_{i=1}^M x_M - \frac{1}{N-M} \sum_{i=M+1}^N x_{M+1} \right) \quad (\text{because } x_i \geq x_{i+1}) \\
&= \frac{N-M}{N} (x_M - x_{M+1}) \\
&\geq 0,
\end{aligned}$$

thus, we obtain  $\frac{1}{M} \sum_{i=1}^M x_i - \frac{1}{N} \sum_{i=1}^N x_i \geq 0$ , that is,  $\frac{1}{M} \sum_{i=1}^M x_i \geq \frac{1}{N} \sum_{i=1}^N x_i$ .  $\blacksquare$

**Property 2** *If  $U_1$  can generate any  $N$ -qubit pure state that is a superposition of at most  $K$  computational basis states, then for any  $|\phi\rangle$ , there exists an SEA output state  $|\psi\rangle$  with  $F(|\phi\rangle, |\psi\rangle) \geq \min\{\frac{K}{r}, 1\}$ , where  $F(|\phi\rangle, |\psi\rangle)$  is the fidelity between  $|\phi\rangle$  and  $|\psi\rangle$ , and  $r$  is the Schmidt rank of  $|\phi\rangle$ .*

**Proof** For any  $2N$ -qubit target state  $|\phi\rangle = \sum_{k=0}^{r-1} \lambda_k |v_k\rangle_A |v_k\rangle_B$ , we explicitly construct an SEA, such that  $|\psi\rangle = S(\hat{\theta})|0\rangle^{\otimes 2N}$  and  $F(|\phi\rangle, |\psi\rangle) \geq \min\{\frac{K}{r}, 1\}$ , where  $\hat{\theta} = \{\hat{\theta}_1, \hat{\theta}_2, \hat{\theta}_3\}$  is a certain set of parameters.

Suppose  $\{\lambda_k\}_{k=0}^{r-1}$  is the Schmidt coefficients of  $|\phi\rangle$  sorted in descending order.

Similar to the proof of Property 1, we can choose a certain set of parameters  $\hat{\theta}$  such that

$$U_1(\hat{\theta}_1)|0\rangle_A^{\otimes N} = \frac{1}{\sqrt{M}} \sum_{k=0}^{\min\{K,r\}-1} \lambda_k |k\rangle, \quad (\text{A34})$$

$$U_2(\hat{\theta}_2)|k\rangle_A = |v_k\rangle_A, \quad (\text{A35})$$

$$U_3(\hat{\theta}_3)|k\rangle_B = |v_k\rangle_B, \quad (\text{A36})$$

where  $M = \sum_{k=0}^{\min\{K,r\}-1} \lambda_k^2$ . Then

$$|\psi\rangle = S(\hat{\theta})|0\rangle^{\otimes 2N} = \frac{1}{\sqrt{M}} \sum_{k=0}^{\min\{K,r\}-1} \lambda_k |v_k\rangle_A |v_k\rangle_B.$$

Hence

$$\begin{aligned}
F(|\phi\rangle, |\psi\rangle) &= |\langle\phi|\psi\rangle|^2 \\
&= \left( \frac{1}{\sqrt{M}} \sum_{k=0}^{\min\{K,r\}-1} \lambda_k^2 \right)^2 \\
&= \frac{1}{M} \left( \sum_{k=0}^{\min\{K,r\}-1} \lambda_k^2 \right)^2 \\
&= \sum_{k=0}^{\min\{K,r\}-1} \lambda_k^2 \\
&\geq \frac{\min\{K,r\}}{r} \sum_{k=0}^{r-1} \lambda_k^2 \quad (\text{due to lemma S3}) \\
&= \frac{\min\{K,r\}}{r} \\
&= \min\left\{\frac{K}{r}, 1\right\},
\end{aligned}$$

with equality holds if and only if  $\lambda_i = \lambda_j, \forall i, j = 0, \dots, r-1$ .  $\blacksquare$

**Property 3** *Constructing a  $2N$ -qubit SEA that can generate an arbitrary pure state requires at most  $O(4^N)$  independent parameters.*

**Proof** As has been proved in property 1, SEA composed of a universal Schmidt layer, two local universal  $N$ -qubit PQC and  $N$  CNOTs, can generate an arbitrary pure state. Therefore, the number of independent parameters of this SEA is  $f(N) = 4^N + 2 \times 4^N - 1$ , that is,  $f(N) = O(4^N)$ .

However, the dimension of unitary group of  $2N$ -qubit is  $4^{2N}$ . Thus, a  $2N$ -qubit universal ansatz needs at least  $O(4^{2N})$  independent parameters.  $\blacksquare$



#### IV. PROOF OF PROPERTY 4

**Property 4** For any  $2N$ -qubit Hamiltonian  $H$ , it holds that

$$\min_S \langle 0|^{\otimes 2N} S^\dagger H S |0\rangle^{\otimes 2N} = E_0, \quad (\text{A37})$$

where  $E_0$  is the ground state energy of  $H$  and the optimization is over all unitaries reachable by SEA with  $U_1$  having universal wavefunction expressibility.

**Proof**

A given  $2N$ -qubit Hamiltonian  $H$  can be written as follows according to spectral decomposition:

$$H = \sum_{i=0}^m E_i P_i,$$

where  $\{E_i\}_{i=0}^m$  are eigenvalues of  $H$  such that  $E_0 < E_1 < \dots < E_m$  and  $P_i$  is a projector onto the eigenspace  $V_i$  corresponding to the eigenvalue  $E_i$ . Then given an arbitrary pure state  $|\psi\rangle \in V_0$ , we have

$$H|\psi\rangle = E_0|\psi\rangle.$$

Note that when the optimization is over all unitaries reachable by SEA with  $U_1$  having universal wavefunction expressibility, there exists an  $S$  such that  $|\psi\rangle = S|0\rangle^{\otimes 2N}$ . Therefore,

$$\langle 0|^{\otimes 2N} S^\dagger H S |0\rangle^{\otimes 2N} = \langle \psi | H | \psi \rangle \quad (\text{A38})$$

$$= E_0 \langle \psi | \psi \rangle \quad (\text{A39})$$

$$= E_0. \quad (\text{A40})$$

Since it is trivial that  $\min_S \langle 0|^{\otimes 2N} S^\dagger H S |0\rangle^{\otimes 2N} \geq E_0$ , we have

$$\min_S \langle 0|^{\otimes 2N} S^\dagger H S |0\rangle^{\otimes 2N} = E_0. \quad (\text{A41})$$

■

#### V. SUPPLEMENTARY DESCRIPTION OF EXPERIMENTS

In this section, we present results from supplementary numerical experiments. Table S1 shows the specific calculation method for the numbers of parameters. Fig. S1 displays the results of VQE using the SEA of Schmidt coefficient layer as  $R_y(\theta)^{\otimes 6}$ , entangling layer as 6 CNOTs and the LBC layers as two 6-qubit ALTs. Fig. S2 shows the variance of the largest partial derivative in each sample.

TABLE S1. Comparison of the number of parameters in different ansatzes.  $N$  represents qubit number,  $l_i$  ( $i = 1, 2, 3$ ) is the number of layer of  $U_i$ .

	SEA	ALT	Random
parameter number	$3N + 6(N - 1)l_1$	$2N + 2(2N - 1)l_2$	$2Nl_3$

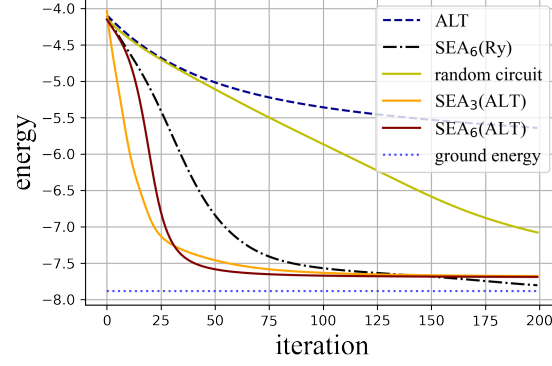


FIG. S1. **Numerical experiment of VQE on LiH (12-qubit).** The blue dotted line is the theoretical ground energy of LiH, and the lines from top to bottom represent the experimental results of ALT, the random circuit, SEA with  $R_y(\theta)$  as  $U_1$  and two ALTs as  $U_2, U_3$  and 6 CNOTs as entangling layer, SEA with three ALTs as  $U_i (i = 1, 2, 3)$  and 3 CNOTs as entangling layer, SEA with three ALTs as  $U_i (i = 1, 2, 3)$  and 6 CNOTs as entangling layer, respectively.  $j (j = 2, 3)$  CNOTs means that we set a composition of  $j$  CNOTs controlled and targeted on the qubit-pairs  $\{(i, N + i)\}_{i=0}^{j-1}$ .

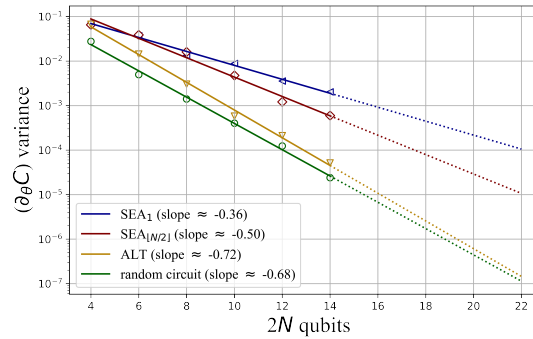


FIG. S2. **Comparison of the scaling of variance between different ansatzes on the Heisenberg model.** It shows the semi-log plot of the variance of the largest partial derivative among parameters in each round of sampling. We ensure different ansatzes have similar number of parameters by setting different depth. The solid part of the fitted lines represents the range we experimented with, while the dotted part represents the expected performance on a larger range.